Design of Dual-Band Coupler With Arbitrary Power Division Ratios and Phase Differences

Pei-Ling Chi, *Member, IEEE*, and Kuan-Lin Ho

***Abstract*—This paper presents, for the first time, a directional coupler that allows for arbitrary power division ratios as well as arbitrary phase differences at dual frequencies of interest. Explicit design equations in terms of dual-band power-dividing ratios and phase differences will be given here and were derived based on the even- and odd-mode decomposition analysis. To illustrate the design procedure, examples will be provided and the relevant studies on the coupler's electrical parameters for a wide range of dual-band specifications and frequency ratios were conducted, by which the graphical solutions can be readily used as the further design tool. In addition, the resulting operational bandwidths are included and discussed for completeness. To validate our idea, four coupler prototypes were carried out according to the given guidelines. Excellent agreement is obtained between the measured and full-wave calculated results. The functional versatility of the proposed simple structure is well suited to applications in dual-band integrated modules, such as the beam-forming networks, for both loss and size reduction.**

***Index Terms*—Arbitrary phase differences, arbitrary power division ratios, directional coupler, dual bands.**

I. Introduction

DIRECTIONAL couplers are one of the most essential building components in the modern communication systems. In this respect, coupler developments in various aspects of applications have been extensively explored over the decades. In general, the improved functionality or performance with size reduction [1], [2], dual-band or multi-band operation [3]–[9], or bandwidth enhancement [10] is of great interest. On the other hand, the practicability of unequal power division between output ports renders a useful solution for intentional power distribution or power compensation in antenna/circuit feeding networks [11]–[15]. Additionally, the coupler design that features filtering and power splitting/combining in a single unit can reduce the number of circuit components and thus occupy less space [16], [17].

Recently, the coupler's ability to produce an arbitrary phase difference between the through and coupled ports [18], and moreover, to combine the flexibility of an arbitrary power division ratio [19]–[23] finds promising applications in many fields. For example, the reflectometer is able to attain optimum design condition by use of hybrid couplers with nonstandard phase differences [24], [25]. Besides, the phase shifters may be removed in conventional beam-forming networks, such as in the Butler matrix [26], [27], where the phase shift can be incorporated into the developed couplers or crossovers with arbitrary phase differences or output phases [22]. In [18], the coupler with arbitrary phase differences was proposed while its fixed (3 dB) power division limits the usage applications. In the follow-up comments on the same coupler, the capability of arbitrary coupling level was supplemented [19]. However, the phase difference concerned herein [19] only ranges from 0° to 90° for the same port excitation, which, in reality, can be extended to an arbitrary value between 0°–360° and will be considered in this presented work. Similarly, the coupler structure in [20] fails to discuss the feasibility of any phase difference other than the value between 0°–90°. In addition, in order to realize arbitrary phase differences, a patterned ground plane is needed in the circular sector patch coupler where a systematic design approach is not available [21]. The use of lumped elements contributes to considerable size reduction, but prevents the coupler prototype from high-frequency applications [22], [23]. Note that, so far in the literature, the coupler functionality having an arbitrary power division and arbitrary phase difference is limited to single-band operation and less effort was made on coupler development with such capability at dual frequencies.

To this end, a single-layer and simple coupler structure is presented and developed in this paper. The even- and odd-mode decomposition technique was applied for coupler analysis. In order to perform dual-band operation, the π network was used to design the constituent transmission lines of arbitrary impedance and phase variations in dual bands of interest. The closed-form design equations will be given in terms of the power division ratios and phase differences in dual bands. Furthermore, the coupler's ability to realize nonstandard phase differences defined between 0°–360° (not including 0°/360° and 180°) will be emphasized and discussed in detail. This paper is organized as follows. In Sections II-A and II-B, the operating principle as well as the dual-band realization of the proposed coupler will be presented where the explicit formulas and a systematic design guideline are included to attempt arbitrary power division ratios and arbitrary phase differences in dual bands. Later, examples are given to illustrate the design procedure and the various investigations on the coupler's electrical parameters and operational bandwidths versus a wide range of dual-band

Manuscript received May 20, 2014; revised September 08, 2014; accepted October 12, 2014. Date of publication October 30, 2014; date of current version December 02, 2014. This work was supported in part by the Ministry of Science and Technology of Taiwan under Grant MOST 103-2221-E-009-032.

P.-L. Chi is with the Department of Electrical and Computer Engineering, National Chiao Tung University, Hsinchu 300, Taiwan (e-mail: peilingchi@nctu.edu.tw).

K.-L. Ho was with the Department of Electrical and Computer Engineering, National Chiao Tung University, Hsinchu 300, Taiwan. He is now with Garmin Inc., New Taipei City 221, Taiwan.

Color versions of one or more of the figures in this paper are available online at http://ieeexplore.ieee.org.

Digital Object Identifier 10.1109/TMTT.2014.2364218

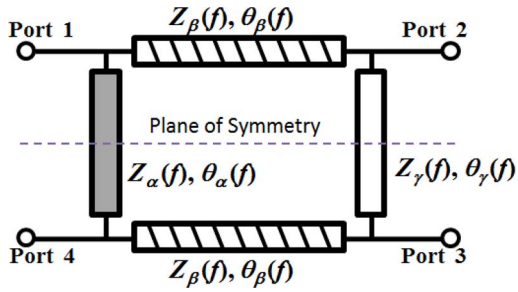

Fig. 1. Schematic representation of the proposed coupler with arbitrary power division ratios and phase differences at dual frequencies.

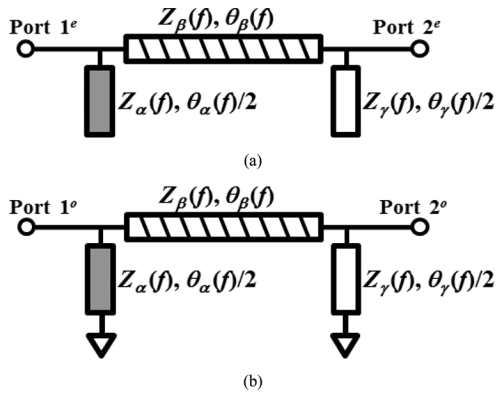

Fig. 2. (a) Even-mode and (b) odd-mode half circuits for analysis of the proposed coupler.

specifications were conducted in Section II-C. In Section III, four dual-band coupler prototypes were developed, fabricated, and characterized by experiments. The experimental results, including the magnitude and phase responses, will be carefully compared to the full-wave calculated counterparts. Finally, a conclusion is drawn in Section IV.

II. Analysis and Implementation of the Dual-Band Coupler

A. Operating Principle

The schematic illustration of the proposed coupler with arbitrary power division ratios and phase differences in dual bands is shown in Fig. 1. The presented coupler is composed of four branch-line elements, including a transmission-line element of impedance $Z_\alpha(f)$ and electrical length $\theta_\alpha(f)$ between ports 1 and 4, a transmission-line element of impedance $Z_\gamma(f)$ and electrical length $\theta_\gamma(f)$ between ports 2 and 3, and a pair of identical line elements of impedance $Z_\beta(f)$ and electrical length $\theta_\beta(f)$. Thus, as can be seen, the structure is symmetric across the midplane and can be analyzed by the even- and odd-mode decomposition technique with the half circuits shown in Fig. 2. Note that each transmission-line element here is responsible for dual-band (designated as f_1 and f_2) implementation, which requires that both of its impedance and electrical length be flexibly engineered at dual frequencies of interest. Thus, the impedance Z_i and phase θ_i ($i = \alpha, \beta$, or γ) are functions of frequency and the π network will be applied for developing such a line prototype. This realization will be detailed in Section II-B. Without loss of generality, if port 1 is designated as the input port, ports 3 and 4 are the outputs of the coupled and through arms, respectively, while port 2 will be the isolated port. Therefore, the power division ratio $K(f)$ and the output phase difference $\varphi(f)$ are defined as the power-split difference and phase difference, respectively, between ports 4 and 3 when port 1 is excited,

$$K(f) = \left|\frac{S_{41}}{S_{31}}\right|^2 \tag{1}$$

$$\varphi(f) = \angle S_{41} - \angle S_{31}. \tag{2}$$

As addressed previously, the proposed coupler is intended to realize arbitrary output parameters K and φ in dual bands of interest, and for design purposes, the mathematical relations in terms of the coupler's electrical parameters will be derived hereafter.

Referring to Fig. 2, the transmission characteristics of the even or odd mode can be conveniently computed by using the transmission $(ABCD)$ matrix, which is the product of the matrices representing the individual sub-circuits

$$\begin{bmatrix} A_{e,o} & B_{e,o} \\ C_{e,o} & D_{e,o} \end{bmatrix} = \begin{bmatrix} 1 & 0 \\ Y_\alpha^{e,o} & 1 \end{bmatrix} \begin{bmatrix} \cos\theta_\beta & jZ_\beta \sin\theta_\beta \\ \dfrac{j\sin\theta_\beta}{Z_\beta} & \cos\theta_\beta \end{bmatrix} \times \begin{bmatrix} 1 & 0 \\ Y_\gamma^{e,o} & 1 \end{bmatrix} \tag{3a}$$

$$Y_{\alpha,\gamma}^e = j\frac{\tan\left(\dfrac{\theta_{\alpha,\gamma}}{2}\right)}{Z_{\alpha,\gamma}} \tag{3b}$$

$$Y_{\alpha,\gamma}^o = -j\frac{\cot\left(\dfrac{\theta_{\alpha,\gamma}}{2}\right)}{Z_{\alpha,\gamma}} \tag{3c}$$

where e or o stands for the even or odd mode, respectively. Note that the frequency dependence is omitted for simplicity, but will not affect the outcome conditions required for proper dual-band operation. Once the $ABCD$ parameters of the two-port even- and odd-mode networks are obtained, the corresponding reflection $(\Gamma_{e,o})$ and transmission $(\mathrm{T}_{e,o})$ coefficients can be readily calculated by conversion between network parameters [28]. Finally, the S -parameters of the coupler are related to the even- and odd-mode reflection and transmission coefficients as follows:

$$S_{11} = \frac{\Gamma_e + \Gamma_o}{2} \tag{4a}$$

$$S_{21} = \frac{\mathrm{T}_e + \mathrm{T}_o}{2} \tag{4b}$$

$$S_{31} = \frac{\mathrm{T}_e - \mathrm{T}_o}{2} \tag{4c}$$

$$S_{41} = \frac{\Gamma_e - \Gamma_o}{2}. \tag{4d}$$

To realize all-port matching and perfect isolation, the conditions that $S_{11} = S_{22} = 0$ and $S_{21} = 0$ must be satisfied at either frequency, which lead to the relations as follows:

$$\mathrm{T}_e = -\mathrm{T}_o \tag{5a}$$
$$\Gamma_e = -\Gamma_o. \tag{5b}$$

According to (5), the $ABCD$ parameters of the even- and odd-mode half circuits can be related as follows:

$$A_e + D_e = -(A_o + D_o) \tag{6a}$$
$$\frac{B_e}{Z_0} + Z_0 C_e = -\left(\frac{B_o}{Z_0} + Z_0 C_o\right) \tag{6b}$$
$$A_e - D_e = A_o - D_o \tag{6c}$$
$$\frac{B_e}{Z_0} - Z_0 C_e = \frac{B_o}{Z_0} - Z_0 C_o \tag{6d}$$

where Z_0 is the port (reference) impedance. In particular, from (6c), the following equation can be derived:

$$Z_\alpha \sin\theta_\alpha = Z_\gamma \sin\theta_\gamma. \tag{7}$$

Thus, if Z_γ is chosen equal to Z_α, the phase relation between θ_α and θ_γ can be deduced as follows:

$$\theta_\gamma = (2n+1)\pi - \theta_\alpha, \qquad \text{if } Z_\alpha = Z_\gamma \tag{8}$$

where n is a non-negative integer ($n = 0, 1, 2, \ldots$). Note that, the other phase solution $\theta_\gamma = 2n\pi + \theta_\alpha$ is disregarded in that the resulting phase difference φ will reduce to only odd multiples of 90° after a further analysis and thus is not considered here for arbitrary phase engineering. Next, the phase θ_β can be solved from (6d) with (8),

$$\theta_\beta = \frac{(2m+1)\pi}{2}, \qquad \text{where } m = 0, 1, 2, \ldots. \tag{9}$$

For size reduction, $\theta_\beta = 90°$ is preferred and will be chosen for phase implementation with $0° < \varphi < 180°$. On the other hand, for the realization with $\varphi > 180°$, it can be shown that $\theta_\beta = 270°$ will be needed. In addition, the impedance Z_α can be related to Z_β by using (6b) in conjunction with the results in (8) and (9),

$$Z_\alpha^2 = \frac{Z_\beta^2}{1 + \left(\frac{Z_\beta}{Z_0}\right)^2}. \tag{10}$$

It can be verified that (6a) still holds with the solutions given in (8)–(10). Thus, the power division ratio K and the phase difference φ, which are already defined in (1) and (2), can be expressed in terms of the above-mentioned parameters as follows:

$$K = \left(\frac{Z_\beta}{Z_0}\right)^2 \csc^2\varphi \tag{11}$$
$$\varphi = \tan^{-1}\left(-\frac{Z_\alpha}{Z_0}\tan\theta_\alpha\right) = \tan^{-1}\left(\frac{Z_\alpha}{Z_0}\tan\theta_\gamma\right). \tag{12}$$

From a design perspective, given the power division ratio K and the phase difference φ at either frequency of dual-band scheme, the six electrical parameters of the coupler schematic in Fig. 1 can be computed as follows:

$$Z_\alpha = Z_\gamma = Z_0\sqrt{\frac{K\sin^2\varphi}{1 + K\sin^2\varphi}} \tag{13}$$
$$Z_\beta = Z_0\sqrt{K}|\sin\varphi| \tag{14}$$
$$\theta_\alpha = \begin{cases} \pi - \tan^{-1}\left(\dfrac{Z_0\tan\varphi}{Z_\alpha}\right), & \text{if } \tan\varphi > 0 \\ -\tan^{-1}\left(\dfrac{Z_0\tan\varphi}{Z_\alpha}\right), & \text{if } \tan\varphi < 0 \end{cases} \tag{15}$$
$$\theta_\gamma = \begin{cases} \tan^{-1}\left(\dfrac{Z_0\tan\varphi}{Z_\alpha}\right), & \text{if } \tan\varphi > 0 \\ \pi + \tan^{-1}\left(\dfrac{Z_0\tan\varphi}{Z_\alpha}\right), & \text{if } \tan\varphi < 0 \end{cases} \tag{16}$$
$$\theta_\beta = \begin{cases} \dfrac{\pi}{2} & \text{if } 0 < \varphi < \pi \\ \dfrac{3\pi}{2}, & \text{if } \pi < \varphi < 2\pi. \end{cases} \tag{17}$$

Note that, for reduced length and better bandwidth, the phase values are chosen as small as possible. Given the power division ratio K and phase difference φ at either operating frequency f_1 or f_2, the corresponding impedances and electrical lengths of the three transmission-line elements in Fig. 1 can be obtained according to (13)–(17). Furthermore, by inspection of (15)–(17), several important observations can be found as follows.

1) Compared to the case with a phase difference φ, the values θ_α and θ_γ are interchanged when designing the phase difference $\pi - \varphi$. Thus, if a phase difference δ is defined as $\delta = \angle S_{32} - \angle S_{42}$, it can be easily shown that $\delta = \pi - \varphi$. In other words, in Fig. 1, the phase differences φ and δ measured at ports 1 and 2, respectively, are supplementary angles. In [18] and [19], such a particular phase relation was illustrated by calculated/experimental results, but analytical explanation is not available therein.
2) The electrical parameters for the case with a phase difference $\varphi > 180°$ are identical to those of the counterpart having the same power division ratio K and phase difference $\varphi - \pi$, except that the electrical length θ_β is increased by 180° ($\theta_\beta = 270°$).
3) The proposed structure is unable to realize the in-phase ($\varphi = 0°$ or 360°) or antiphase (180°) phase difference given that port 2 is the isolated port when port 1 is excited. Instead, if port 3 is defined as the isolated port, such a phase difference is feasible between ports 2 and 4, as was presented in [15].

B. Dual-Band Implementation

As can be observed from (13) and (14), the impedance of each transmission-line element in the coupler may be different accordingly at dual frequencies to fulfill arbitrary power division ratios and phase differences. Thus, the π network is applied

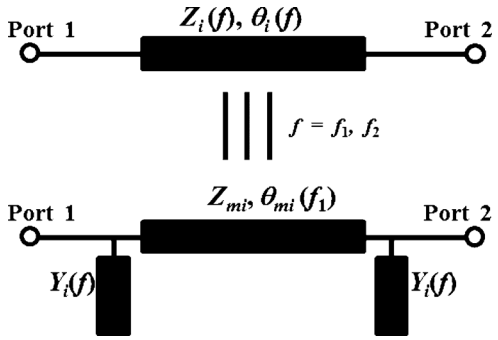

Fig. 3. π network for implementing a transmission-line element of effective impedance $Z_i(f)$ and electrical length $\theta_i(f)$.

to implement each line element in Fig. 1. As shown in Fig. 3, the π network consists of a host transmission line of characteristic impedance Z_{mi} and electrical length θ_{mi} (evaluated at the lower frequency f_1), and two identical open stubs loaded at both ends. The parameter $Y_i(f)$ represents the admittance of the open stubs. Thus, at operational frequencies f_1 and f_2, the $ABCD$ parameters of the original line element must equate to those of the π network as follows:

$$\begin{bmatrix} \cos\theta_i(f_1) & jZ_i(f_1)\sin\theta_i(f_1) \\ \dfrac{j\sin\theta_i(f_1)}{Z_i(f_1)} & \cos\theta_i(f_1) \end{bmatrix} = \begin{bmatrix} 1 & 0 \\ Y_i(f_1) & 1 \end{bmatrix} \begin{bmatrix} \cos\theta_{mi} & jZ_{mi}\sin\theta_{mi} \\ \dfrac{j\sin\theta_{mi}}{Z_{mi}} & \cos\theta_{mi} \end{bmatrix} \begin{bmatrix} 1 & 0 \\ Y_i(f_1) & 1 \end{bmatrix} \tag{18a}$$

$$\begin{bmatrix} \cos\theta_i(f_2) & jZ_i(f_2)\sin\theta_i(f_2) \\ \dfrac{j\sin\theta_i(f_2)}{Z_i(f_2)} & \cos\theta_i(f_2) \end{bmatrix} = \begin{bmatrix} 1 & 0 \\ Y_i(f_2) & 1 \end{bmatrix} \begin{bmatrix} \cos(M\theta_{mi}) & jZ_{mi}\sin(M\theta_{mi}) \\ \dfrac{j\sin(M\theta_{mi})}{Z_{mi}} & \cos(M\theta_{mi}) \end{bmatrix} \times \begin{bmatrix} 1 & 0 \\ Y_i(f_2) & 1 \end{bmatrix} \tag{18b}$$

where $M = f_2/f_1$. Note that $\theta_i(f_1), \theta_i(f_2), Z_i(f_1)$, and $Z_i(f_2)$ represent the prior known parameters for any line elements in the coupler and can be readily obtained from (13)–(17) as soon as the values of $K(f_1), K(f_2), \varphi(f_1)$ and $\varphi(f_2)$ are specified. Thus, $\theta_{mi}, Z_{mi}, Y_i(f_1)$, and $Y_i(f_2)$ can be solved as follows:

$$\frac{\sin(M\theta_{mi})}{\sin\theta_{mi}} = \frac{Z_i(f_2)\sin\theta_i(f_2)}{Z_i(f_1)\sin\theta_i(f_1)} \tag{19}$$

$$Z_{mi} = \frac{Z_i(f_1)\sin\theta_i(f_1)}{\sin\theta_{mi}} \tag{20}$$

$$Y_i(f_1) = j\left[\frac{\cos\theta_{mi} - \cos\theta_i(f_1)}{Z_i(f_1)\sin\theta_i(f_1)}\right] \tag{21}$$

$$Y_i(f_2) = j\left[\frac{\cos(M\theta_{mi}) - \cos\theta_i(f_2)}{Z_i(f_2)\sin\theta_i(f_2)}\right]. \tag{22}$$

By replacing each transmission-line element in Fig. 1 with the corresponding π network, the proposed dual-band coupler is illustrated in Fig. 4(a) where the previously calculated parameters

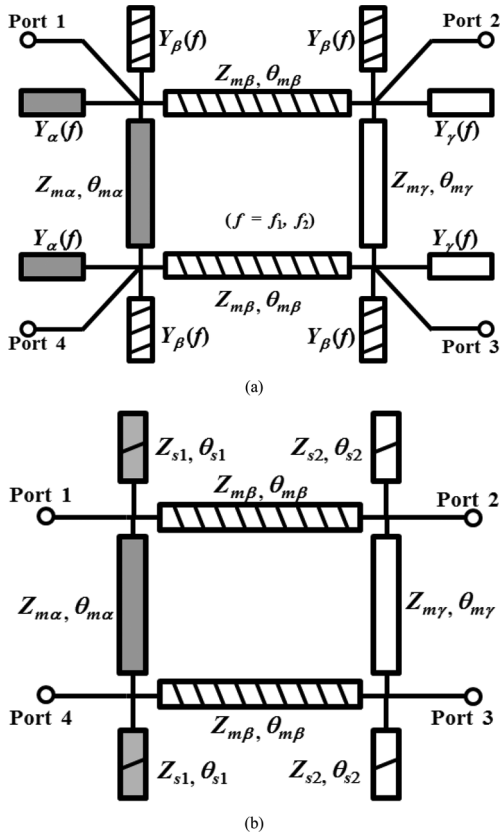

Fig. 4. (a) Configuration and (b) realized prototype of the proposed dual-band coupler based on the π networks. All electrical lengths are evaluated at f_1.

Z_{mi}, θ_{mi}, and $Y_i(f)$ ($i = \alpha, \beta$, or γ) are indicated. To facilitate fabrication, each pair of loaded stubs at the same vertex was implemented as a single open stub, as shown in Fig. 4(b). Thus, the realized coupler prototype comprises two kinds of open stubs with characteristic impedances Z_{s1} and Z_{s2} and electrical lengths θ_{s1} and θ_{s2}, and can be determined by $Y_i(f_1)$ and $Y_i(f_2)$ in (21) and (22) as follows:

$$\frac{\tan(M\theta_{s1})}{\tan\theta_{s1}} = \frac{Y_\alpha(f_2) + Y_\beta(f_2)}{Y_\alpha(f_1) + Y_\beta(f_1)} \tag{23}$$

$$Z_{s1} = j\left[\frac{\tan\theta_{s1}}{Y_\alpha(f_1) + Y_\beta(f_1)}\right] \tag{24}$$

$$\frac{\tan(M\theta_{s2})}{\tan\theta_{s2}} = \frac{Y_\gamma(f_2) + Y_\beta(f_2)}{Y_\gamma(f_1) + Y_\beta(f_1)}, \tag{25}$$

$$Z_{s2} = j\left[\frac{\tan\theta_{s2}}{Y_\gamma(f_1) + Y_\beta(f_1)}\right]. \tag{26}$$

C. Examples and Design Procedure

Having formulated coupler design in the previous sections, two examples are given here for demonstration purposes. The first coupler is designed at $f_1 = 2.4$ GHz and $f_2 = 5.2$ GHz (the frequency ratio $M = 5.2/2.4$) with $K(f_1) = 8, \varphi(f_1) = 60^\circ$ and $K(f_2) = 4, \varphi(f_2) = 75^\circ$. According to the specification, Table I gives the corresponding dual-band parameters for the transmission-line elements in Fig. 1 using (13)–(17). Subsequently, by resorting to (19)–(26) with the data in Table I, the

TABLE I
CALCULATED PARAMETERS FOR THE TRANSMISSION-LINE ELEMENTS IN THE COUPLER GIVEN THE DIVISION RATIOS $K(f_1) = 8, K(f_2) = 4$, AND PHASE DIFFERENCES $\varphi(f_1) = 60°, \varphi(f_2) = 75°$

	f_1	f_2
$K(f)$	8	4
$\varphi(f)$	60°	75°
$Z_\alpha(f)$	46.29 Ω	44.40 Ω
$\theta_\alpha(f)$	118.13°	103.39°
$Z_\beta(f)$	122.47 Ω	96.59 Ω
$\theta_\beta(f)$	90°	90°
$Z_\gamma(f)$	46.29 Ω	44.40 Ω
$\theta_\gamma(f)$	61.87°	76.61°

TABLE II
CIRCUIT PARAMETERS FOR THE PROPOSED DUAL-BAND ($f_2/f_1 = M = 5.2/2.4$) COUPLER WITH SPECIFICATIONS GIVEN IN TABLE I (ALL ELECTRICAL LENGTHS ARE EVALUATED AT 2.4 GHz)

$Z_{m\alpha}$	$Z_{m\beta}$	$Z_{m\gamma}$	Z_{s1}	Z_{s2}
49.70 Ω	138 Ω	49.70 Ω	68.25 Ω	177 Ω
$\theta_{m\alpha}$	$\theta_{m\beta}$	$\theta_{m\gamma}$	θ_{s1}	θ_{s2}
55.22°	62.56°	55.22°	63.42°	47.60°

TABLE III
CALCULATED PARAMETERS FOR THE TRANSMISSION-LINE ELEMENTS IN THE COUPLER GIVEN THE DIVISION RATIOS $K(f_1) = 4, K(f_2) = 4$, AND PHASE DIFFERENCES $\varphi(f_1) = 60°, \varphi(f_2) = 60°$

	f_1	f_2
$K(f)$	4	4
$\varphi(f)$	60°	60°
$Z_\alpha(f)$	43.30 Ω	43.30 Ω
$\theta_\alpha(f)$	116.57°	116.57°
$Z_\beta(f)$	86.60 Ω	86.60 Ω
$\theta_\beta(f)$	90°	90°
$Z_\gamma(f)$	43.30 Ω	43.30 Ω
$\theta_\gamma(f)$	63.43°	63.43°

TABLE IV
CIRCUIT PARAMETERS FOR THE PROPOSED DUAL-BAND ($f_2/f_1 = M = 5.2/2.4$) COUPLER WITH SPECIFICATIONS GIVEN IN TABLE III (ALL ELECTRICAL LENGTHS ARE EVALUATED AT 2.4 GHz)

$Z_{m\alpha}$	$Z_{m\beta}$	$Z_{m\gamma}$	Z_{s1}	Z_{s2}
46.26 Ω	103.45 Ω	46.26 Ω	75.37 Ω	125 Ω
$\theta_{m\alpha}$	$\theta_{m\beta}$	$\theta_{m\gamma}$	θ_{s1}	θ_{s2}
56.84°	56.84°	56.84°	67.47°	48.02°

electrical parameters for the realized prototype in Fig. 4(b) can be obtained and are given in Table II. Similarly, the second coupler is operated at 2.4 and 5.2 GHz with $K(f_1) = 4, \varphi(f_1) = 60°$ and $K(f_2) = 4, \varphi(f_2) = 60°$. Tables III and IV present the calculated results. In particular, since $Z_\alpha = Z_\gamma$ and $\theta_\alpha + \theta_\gamma = \pi$, by (19) and (20), it can be shown that $Z_{m\alpha} = Z_{m\gamma}$ and $\theta_{m\alpha} = \theta_{m\gamma}$, as are seen in Tables II and IV. Additionally, in Tables I and III, the impedance Z_β in either case is notably higher than the impedance Z_α or Z_γ, and is resulted from the

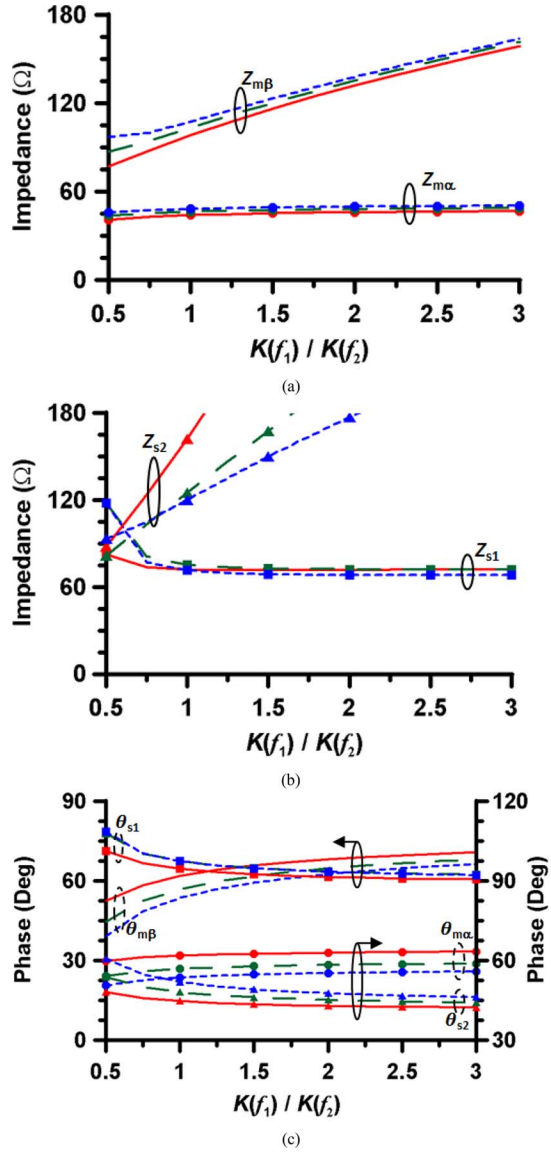

Fig. 5. (a) Host-line impedances, (b) stub-line impedances, and (c) host-line and stub-line electrical lengths against the ratio $K(f_1)/K(f_2)$ when $K(f_2) = 4, \varphi(f_1) = 60°, f_1 = 2.4$ GHz and $f_2 = 5.2$ GHz. Three phase cases corresponding to $\varphi(f_2) = 45°, 60°$, and $75°$ are illustrated by the solid curve, long dashed curve, and short dashed curve, respectively. The phase solutions for $\theta_{m\alpha}, \theta_{m\beta}, \theta_{s1}$, and θ_{s2} are represented by the curves with circle symbol, no symbol, square symbol, and triangle symbol, respectively.

high power division ratios specified in dual bands. By inspection of (13) and (14), when the power ratio K is large at a frequency, the impedance Z_β will increase accordingly and Z_α or Z_γ will approach Z_0, typically 50 Ω. As a consequence, by (20), the host line impedance $Z_{m\beta}$ in the π network is usually higher than the counterpart $Z_{m\alpha}$ or $Z_{m\gamma}$. This inference can be validated from the diagrams in Fig. 5 where the impedances of the host lines as well as the open stubs are considered with respect to the ratio $K(f_1)/K(f_2)$ when $K(f_2)$ is fixed as 4. In this study, the frequency ratio $M = 5.2/2.4$. Note that three dual-band phase differences of $(\varphi(f_1), \varphi(f_2)) = (60°, 45°), (60°, 60°)$, and $(60°, 75°)$ are considered and illustrated here. From Fig. 5(a), it can be observed that $Z_{m\beta}$ under consideration increases with the power division ratio $K(f_1)$

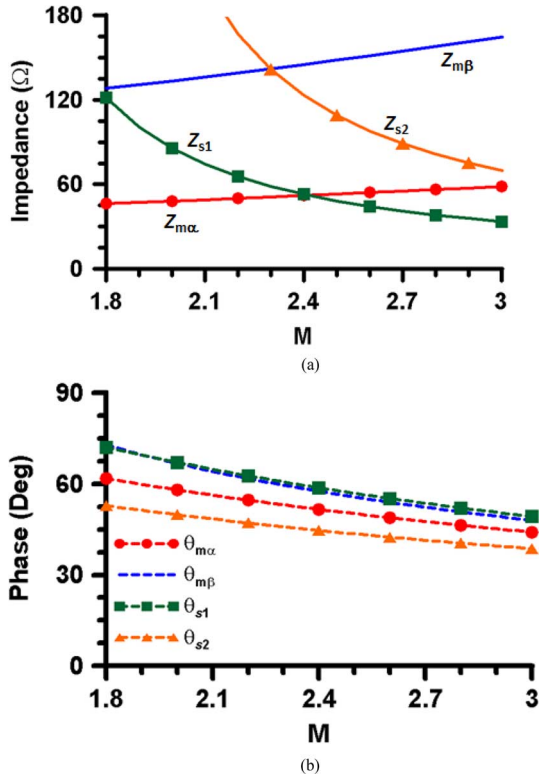

Fig. 6. (a) Impedances and (b) phases of the host lines and stub lines against the frequency ratio M when $K(f_1) = 8, \varphi(f_1) = 60°, K(f_2) = 4$, and $\varphi(f_2) = 75°$.

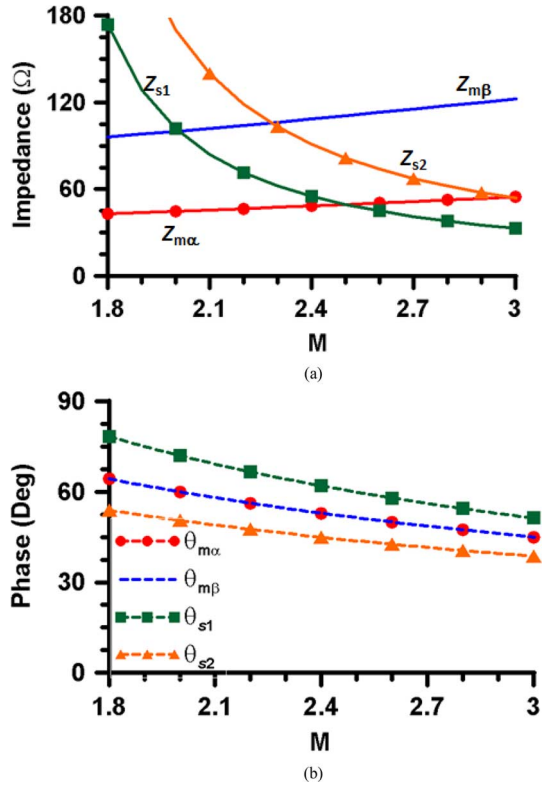

Fig. 7. (a) Impedances and (b) phases of the host lines and stub lines against the frequency ratio M when $K(f_1) = 4, \varphi(f_1) = 60°, K(f_2) = 4$, and $\varphi(f_2) = 60°$.

for all cases while $Z_{m\alpha}$ $(= Z_{m\gamma})$ remains relatively constant around 50 Ω. Furthermore, as the power ratio $K(f_1)$ increases, in Fig. 5(b) the impedance Z_{s2} of the open stub is remarkably increased, which then determines the attainable power division ratio for the proposed dual-band coupler based on the π networks. For the prototype built on a RO4003C substrate of thickness 1.5 mm and of dielectric constant 3.38, the maximum achievable impedance is about 180 Ω for a 0.1-mm line width. Thus, the maximum impedance scale is limited to 180 Ω throughout this paper to better clarify the feasible power and phase applications or the attainable frequency ratio in the dual-band scheme. Based on the results shown in Fig. 5(b), the maximum realizable power division ratio $K(f_1)$ is about 1.13×4, 1.75×4, and 2.0×4, respectively, for $\varphi(f_2) = 45°, 60°$, and $75°$. The corresponding phase solutions for the host and stub lines are shown in Fig. 5(c). From Fig. 5(c), while less variation is observed for the electrical length $\theta_{m\alpha}$, the phase $\theta_{m\beta}$ is gradually increased against the ratio of dual-band power divisions, indicating that an increased coupler size, defined as the area enclosed by the host lines of $Z_{m\alpha}$ and $Z_{m\beta}$ $(\theta_{m\alpha} \times \theta_{m\beta})$, is needed. Furthermore, when the phase varies from $\varphi(f_2) = 75°$ to $\varphi(f_2) = 45°$, both $\theta_{m\alpha}$ and $\theta_{m\beta}$ are increased and this results in a larger footprint. Note that the impedance and phase values of the examples presented in Tables II and IV can be obtained from Fig. 5 for $K(f_1)/K(f_2) = 2, \varphi(f_2) = 75°$ and $K(f_1)/K(f_2) = 1, \varphi(f_2) = 60°$, respectively.

On the other hand, the variations of the coupler's electrical parameters versus the frequency ratio M, with a variation step of 0.1, are investigated. Figs. 6 and 7 show the calculated results for $K(f_1) = 8, \varphi(f_1) = 60°, K(f_2) = 4, \varphi(f_2) = 75°$ and for $K(f_1) = 4, \varphi(f_1) = 60°, K(f_2) = 4, \varphi(f_2) = 60°$, respectively. It can be observed that as M increases, the stub impedances and all electrical lengths are reduced, except the host-line impedances. Particularly, as M becomes small, the stub impedance Z_{s2} increases rapidly (as compared to Z_{s1}) and thus predominates the minimum attainable frequency ratio of dual-band operation based on the proposed architecture. From Figs. 6 and 7, it can be read that the minimum achievable ratio is about 2.2 and 2.0, respectively, for the first and second cases. Thus, the minimum obtainable dual-frequency separation is varied from case to case and is determined by particular realizations of power ratios and phase differences. According to the above observations, to improve design flexibility of the dual-band coupler in terms of arbitrary operational frequencies or closer band separation, arbitrary power divisions, and phase differences, some auxiliary techniques that enable microstrip lines to be realized with high impedance can be applied at the expense of fabrication complexity such as the microstrip line with the defected ground structure [29] and the surface-mount inductor-loaded line section [30]. Furthermore, the fractional bandwidths in the respective bands f_1 and f_2 in correspondence with the case shown in Fig. 6 are illustrated in Fig. 8(a). The fractional bandwidth is defined as a frequency range where the return loss and isolation are better than 15 dB ($|S_{11}|, |S_{21}| < -15$ dB), the amplitude imbalance is less than 1 dB ($K(f) \pm 1$ dB), and the phase imbalance is less than 10° ($\varphi(f) \pm 10°$). On the average, the fractional bandwidths are relatively constant over the frequency ratio M in two operational

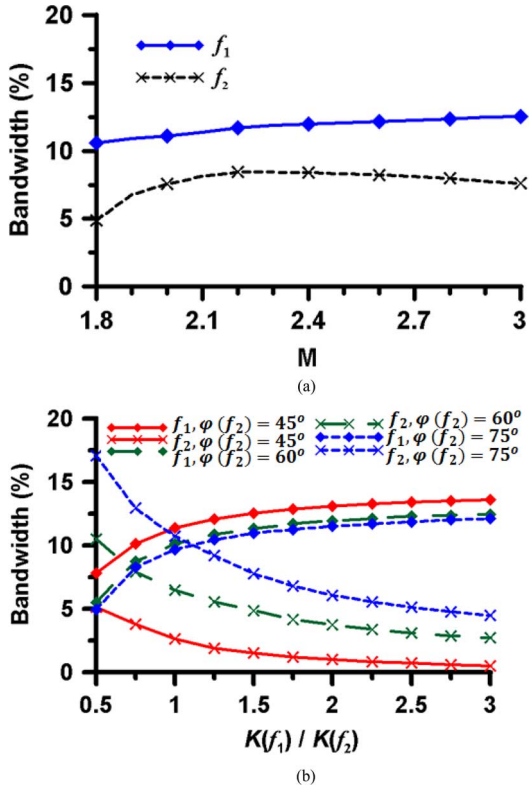

Fig. 8. (a) Fractional bandwidths against the frequency ratio M. The dual-band specification is as follows: $K(f_1) = 8, \varphi(f_1) = 60°, K(f_2) = 4$, and $\varphi(f_2) = 75°$. The lower frequency f_1 was designated as 1 GHz. (b) Fractional bandwidths against the ratio $K(f_1)/K(f_2)$ when $K(f_2) = 4, \varphi(f_1) = 60°, f_1 = 2.4$ GHz and $f_2 = 5.2$ GHz.

TABLE V
DUAL-BAND [$f_1 = 2.4$ GHz AND $f_2 = 5.2$ GHz/5.8 GHz (FOR COUPLER 3 ONLY)] SPECIFICATIONS FOR THE FOUR FABRICATED COUPLERS

Coupler	$K(f_1)$	$K(f_2)$	$\varphi(f_1)$	$\varphi(f_2)$
1	8	4	60^o	75^o
2	4	4	60^o	60^o
3	2	4	90^o	60^o
4	4	2	45^o	90^o

bands. In addition, the fractional bandwidths versus the ratio $K(f_1)/K(f_2)$, corresponding to the case study in Fig. 5, are calculated and shown in Fig. 8(b). For the bandwidths centered at f_2, it is seen that the bandwidths drop considerably with the ratio $K(f_1)/K(f_2)$. Furthermore, it is interesting to note that a tradeoff exists for bandwidth performance between the three phase cases. In other words, the case with $\varphi(f_2) = 45°$ has the wider bandwidth at f_1 while having the narrowest bandwidth in its second band among the three. The reverse situation can be found for the case with $\varphi(f_2) = 75°$.

In short, the design guidelines for the proposed dual-band coupler are summarized as follows.

Step 1) Use (13)–(17) to determine the impedances Z_α $(= Z_\gamma)$ and Z_β, and the electrical lengths $\theta_\alpha, \theta_\beta$, and θ_γ of the transmission-line elements at either frequency once the power division ratios $K(f_1)$ and $K(f_2)$, and phase differences $\varphi(f_1)$ and $\varphi(f_2)$ are specified.

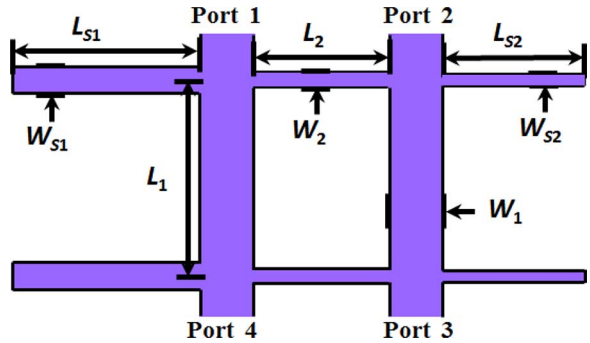

Fig. 9. Physical layout of the proposed coupler with arbitrary power division ratios and phase differences at dual frequencies. The coupler is symmetric across the horizontal midplane.

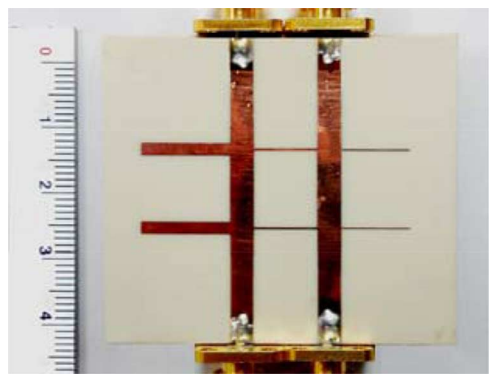

Fig. 10. Photograph of the fabricated dual-band coupler 1.

TABLE VI
DIMENSIONS OF THE FOUR FABRICATED COUPLERS. ALL UNITS ARE IN MILLIMETERS

Coupler	W_1	L_1	W_2	L_2	W_{s1}	L_{s1}	W_{s2}	L_{s2}
1	3.56	12.0	0.29	9.48	1.83	13.2	0.16	10.2
2	3.83	13.5	0.77	9.17	1.62	13.1	0.44	9.58
3	3.38	12.3	0.30	4.67	0.97	14.3	3.52	11.3
4	4.90	11.0	1.55	5.84	1.00	15.5	0.16	12.8

Step 2) Based on the values in Step 1, use (19)–(26) to obtain electrical parameters of the coupler prototype using the π networks, including the host/stub-line impedances $Z_{m\alpha}(= Z_{m\gamma}), Z_{m\beta}, Z_{s1}$, and Z_{s2}, and host/stub-line electrical lengths $\theta_{m\alpha}(= \theta_{m\gamma}), \theta_{m\beta}, \theta_{s1}$, and θ_{s2}.

Step 3) In consideration of the coupler performance, choose appropriate phase solutions. To this end, shorter length is preferred for bandwidth enhancement and size reduction.

III. EXPERIMENTAL AND FULL-WAVE CALCULATED RESULTS

To validate the feasibility of the proposed design concept, four coupler prototypes with prescribed power divisions and phase differences in dual bands were developed, fabricated, and characterized. The dual-band specification for each realization is given in Table V. As can be seen, the presented examples of a variety of power division ratios and phase differences were carried out here. All dual-band couplers were designed at 2.4 and 5.2 GHz, except for coupler 3, which operates at 2.4 and

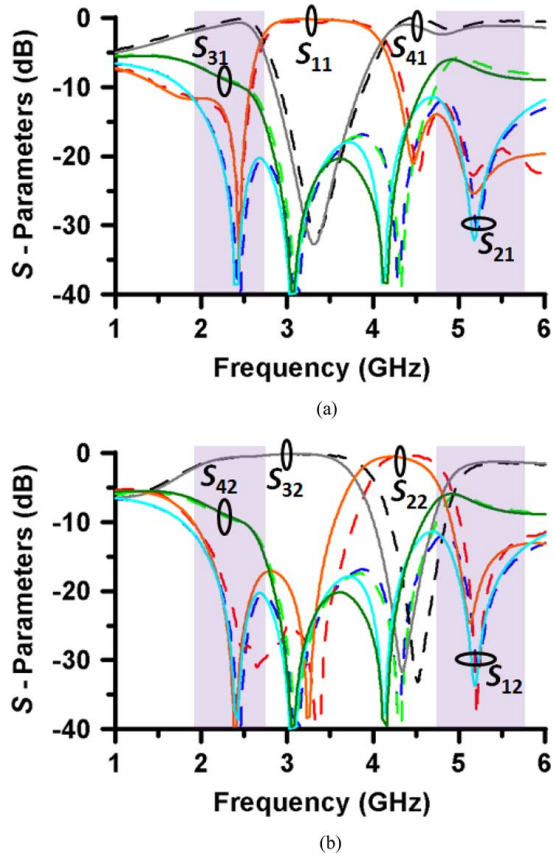

Fig. 11. Measured (dashed lines) and simulated (solid lines) S -parameters of the coupler 1. (a) S -parameters obtained when port 1 is the input port. (b) S -parameters obtained when port 2 is the input port.

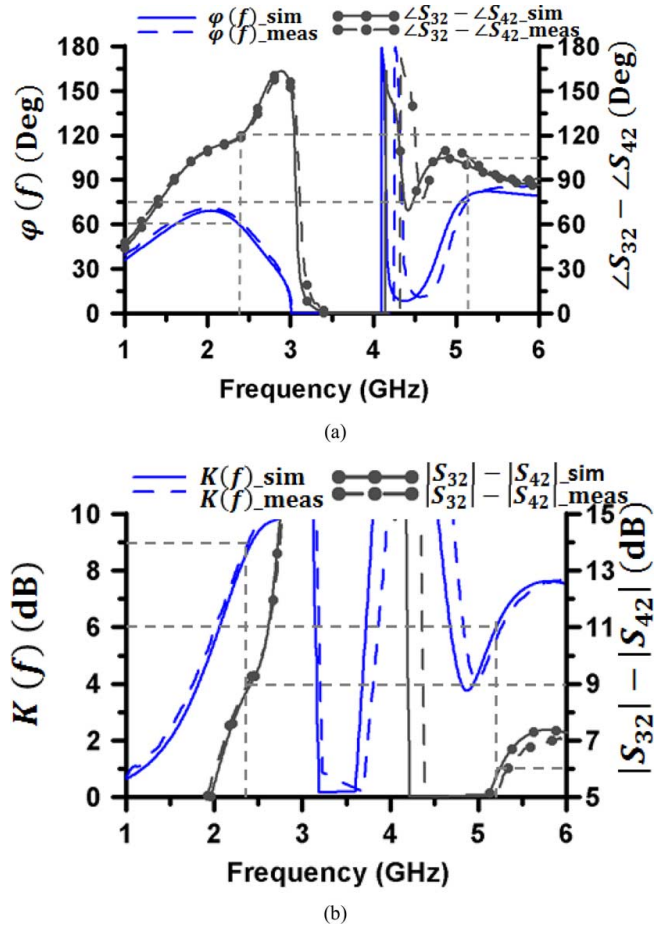

Fig. 12. Measured and simulated: (a) phase differences and (b) power division ratios of coupler 1. The curves without and with the circle symbols represent the results obtained when the input ports are ports 1 and 2, respectively.

5.8 GHz. All couplers were developed on the RO4003C substrates of thickness $h = 1.5$ mm (60 mil) and of dielectric constant $\varepsilon_r = 3.38$. The physical layout of the proposed dual-band coupler is shown in Fig. 9. Note that the coupler is symmetric across the horizontal midplane. When referring to Fig. 4(b), the horizontal lines with width W_2 correspond to the host lines of characteristic impedance $Z_{m\beta}$ while the vertical lines with width W_1 represent the host lines of impedance $Z_{m\alpha}$ $(= Z_{m\gamma})$. In addition, the stub lines with widths W_{s1} and W_{s2} are the open stubs of impedances Z_{s1} and Z_{s2}, respectively. Note that, though not considered in this presented work, size reduction of the proposed dual-band coupler may be achieved by properly folding the host and stub lines [8], configuring the stubs in the area enclosed by the host lines [11], or designing the stepped-impedance host lines [11]. The photograph of the coupler 1 is shown in Fig. 10 and the corresponding physical dimensions, along with those for the other three couplers, can be referred to Table VI. The measured and simulated S-parameters of the coupler 1 are shown in Fig. 11 and are in excellent agreement. The full-wave simulation was carried out in the High Frequency Structure Simulator (HFSS). From Fig. 11, dual-band characteristics at 2.4 and 5.2 GHz are obtained. Furthermore, the experimental results of the power division ratio $K(f)$ as well as the phase difference $\varphi(f)$ are depicted in Fig. 12. It can be observed that the power division ratios of $K(f_1) = 8$ (9 dB) and $K(f_2) = 4$ (6 dB), and the phase differences of $\varphi(f_1) = 60°$ and $\varphi(f_2) = 75°$ are achieved as designed. Moreover, the measured power division ratio $|S_{32}| - |S_{42}|$ and the phase difference $\angle S_{32} - \angle S_{42}$ with port 2 being the input port are included for validation purpose. From Fig. 12(a), it is verified that the sum of the phase difference $\varphi(\angle S_{41} - \angle S_{31})$ and $\angle S_{32} - \angle S_{42}$ is 180° at either frequency, as was explained previously. Furthermore, the power division ratios $|S_{32}| - |S_{42}|$ (the right y-axis) in Fig. 12(b) are 9 dB at 2.4 GHz and 6 dB at 5.2 GHz, which agree with the results obtained for $K(f)$ at the respective frequencies. For better clarity, the detailed coupler performance, including the return loss $|S_{11}|$, isolation $|S_{21}|$, power division ratio $K(f) = |S_{41}| - |S_{31}|$, phase difference $\varphi(f) = \angle S_{41} - \angle S_{31}$, and the corresponding bandwidths, are summarized and given in Table VII. Note that, compared to other results, the measured bandwidths at f_1 for the coupler 4 are, on the average, much smaller and can be attributed to the phase realization $\varphi(f_1) = 45°$. Similar observation is found in Fig. 8(b) where the bandwidths in the second band for $\varphi(f_2) = 45°$ are smaller than the bandwidths for $\varphi(f_2) = 60°$ and 75°. Nevertheless, the feasibility of the proposed design approach for the dual-band coupler prototype with arbitrary power division ratios and phase differences is verified by the experimental results. Moreover, all the relevant works are compared in Table VIII where the coupler's ability to afford dual- or multi-band operation, the circuit configuration to facilitate coupler implementation, and the functional

TABLE VII
EXPERIMENTAL RESULTS OF THE FABRICATED FOUR COUPLERS

Coupler		$\lvert S_{11}\rvert$ (dB)	$\lvert S_{21}\rvert$ (dB)	$K(f)$ (dB)	$\varphi(f)$ (Deg)	BW (%) $\lvert S_{11}\rvert$< -15dB	BW (%) $\lvert S_{21}\rvert$ < -15dB	BW (%) $K(f)$ ± 1dB	BW (%) $\varphi(f)$± 5°
1	f_1	-22.3	-33.6	9.17	61.91	10.79	75.63	14.11	7.84
	f_2	-22.6	-30.2	5.67	79.18	28.57	13.43	7.35	2.92
2	f_1	-29.1	-17.0	5.59	59.92	12.71	55.16	24.09	11.37
	f_2	-26.6	-31.8	5.03	60.81	10.17	25.56	22.10	5.88
3	f_1	-23.6	-22.4	3.87	92.15	18.72	16.38	11.71	15.70
	f_2	-18.1	-16.3	5.21	64.46	35.13	17.15	30.41	15.53
4	f_1	-18.6	-32.1	5.63	48.13	3.31	33.33	4.96	2.90
	f_2	-21.8	-21.8	3.15	90.80	33.92	15.98	10.32	> 39.11

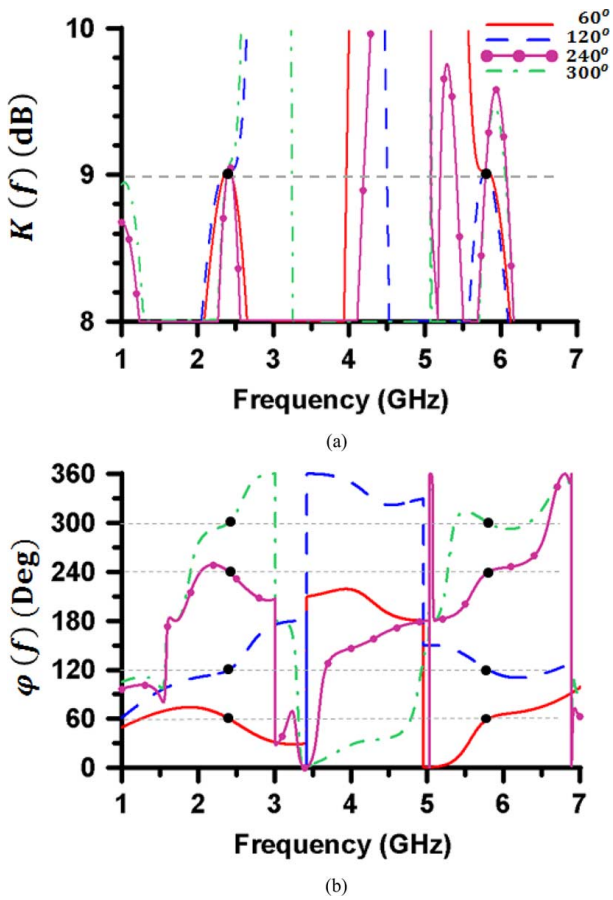

Fig. 13. Simulated results for: (a) power division ratios and (b) phase differences for four coupler designs with $\varphi(f_1) = \varphi(f_2) = 60°, 120°, 240°$, and $300°$, respectively, and $K(f_1) = K(f_2) = 8$ (9 dB) for all cases. The couplers were designed at $f_1 = 2.4$ GHz and $f_2 = 5.8$ GHz.

TABLE VIII
PERFORMANCE COMPARISON FOR THE PROPOSED AND REFERENCE COUPLERS

	Operation	Coupler Configuration	Power Division	Phase Difference
This Work	dual-band	π-network MSL	arbitrary	arbitrary (0°—360°)
[4]	dual-band	π-network MSL	3-dB	90°
[11]	dual-band	stepped-impedance π-network MSL	arbitrary	90°/180°
[18]	single-band	MSL	3-dB	arbitrary (0°—90°)
[19]	single-band	MSL	arbitrary	arbitrary (0°—90°)
[20]	single-band	coupled MSL	arbitrary	arbitrary (0°—90°)
[21]	single-band	MSL with defected ground	arbitrary	arbitrary (0°—180°)
[22]	single-band	SMT	arbitrary	arbitrary (0°—360°)

MSL: microstrip-line technology, SMT: surface-mount technology

flexibility to allow for arbitrary power divisions and arbitrary phase differences defined from 0° to 360° between the outputs are all taken into consideration. Note that in terms of the coupler configuration, similar structures can be found in [4] and [11] where the π-network and the stepped-impedance π-network were, respectively, utilized for compact and dual-band operation. On the other hand, due to the versatile power and phase applications, the π-network in this work is mainly applied for flexibly fulfilling power and phase requirements at dual frequencies of interest. In particular, compared to prior works, this presented coupler is the first realization of a dual-band prototype that attempts both arbitrary power divisions and phase differences. Furthermore, explicit design equations for a non-standard phase difference ranging from 0° to 360° (not applicable to the phases 0°/360° and 180°) are provided for the proposed structure while most of references consider or discuss a limited phase-difference realization, such as from 0° to 90° or from 0° to 180°. To demonstrate the practicability of arbitrary phase difference within 360° based on the presented design guidelines, Fig. 13 shows the simulated results of four coupler prototypes with different phase differences 60°, 120°, 240°, and 300° ($\varphi(f_1) = \varphi(f_2)$) and identical power division ratios $K(f_1) = K(f_2) = 8$ at $f_1 = 2.4$ GHz and $f_2 = 5.8$ GHz. For each coupler, the division ratios of 9 dB as well as identical phase differences (60°–300°) in dual bands were obtained as designed. Note that according to (13) and (14), this presented coupler is unable to realize a phase difference $\varphi = 0°$ (360°) and $\varphi = 180°$ between ports 3 and 4 (see Fig. 1). A further analysis shows that the in-phase or antiphase phase difference can be fulfilled between ports 2 and 4 if ports 1 and 3 are designated as the input and isolated ports, respectively. In [21], to realize the 0°/180° phase differences, different output pairs were used. Nevertheless, it is clear that this work presents, for the first time,

a single-layer structure that exhibits greater design flexibility of the power divisions and phase differences engineering at dual frequencies of interest.

IV. Conclusion

In this paper, the analysis and design of a coupler prototype that allows for arbitrary power divisions and phase differences in dual bands are carried out for the first time and discussed in details. This coupler renders a simple structure with increased functionality such as the dual-band operation and an extended range of phase difference engineering. Good agreement is obtained between the experimental and calculated results.

References

[1] D. I. Kim and G.-S. Yang, "Design of new hybrid-ring directional coupler using $\lambda/8$ or $\lambda/6$ sections," *IEEE Trans. Microw. Theory Techn.*, vol. 39, no. 10, pp. 1779–1784, Oct. 1991.

[2] H. Okabe, C. Caloz, and T. Itoh, "A compact enhanced-bandwidth hybrid ring using an artificial lumped-element left-handed transmission-line section," *IEEE Trans. Microw. Theory Techn.*, vol. 52, no. 3, pp. 798–804, Mar. 2004.

[3] L. K. Yeung, "A compact dual-band 90° coupler with coupled-line sections," *IEEE Trans. Microw. Theory Techn.*, vol. 59, no. 9, pp. 2227–2232, Sep. 2011.

[4] K.-K. M. Cheng and F.-L. Wong, "A novel approach to the design and implementation of dual-band compact planar 90° branch-line coupler," *IEEE Trans. Microw. Theory Techn.*, vol. 52, no. 11, pp. 2458–2463, Nov. 2004.

[5] S. Y. Zheng, S. H. Yeung, W. S. Chan, K. F. Man, S. H. Leung, and Q. Xue, "Dual-band rectangular patch hybrid coupler," *IEEE Trans. Microw. Theory Techn.*, vol. 56, no. 7, pp. 1721–1728, Jul. 2008.

[6] M.-J. Park and B. Lee, "Dual-band, cross coupled branch line coupler," *IEEE Microw. Wireless Compon. Lett.*, vol. 15, no. 10, pp. 655–657, Oct. 2005.

[7] P.-L. Chi and T. Itoh, "Miniaturized dual-band directional couplers using composite right/left-handed transmission structures and their applications in beam pattern diversity systems," *IEEE Trans. Microw. Theory Techn.*, vol. 57, no. 5, pp. 1207–1215, May 2009.

[8] F. Lin, Q.-X. Chu, and Z. Lin, "A novel tri-band branch-line coupler with three controllable operating frequencies," *IEEE Microw. Wireless Compon. Lett.*, vol. 20, no. 12, pp. 666–668, Dec. 2010.

[9] C.-W. Tang and M.-G. Chen, "Design of multipassband microstrip branch-line couplers with open stubs," *IEEE Trans. Microw. Theory Techn.*, vol. 57, no. 1, pp. 196–204, Jan. 2009.

[10] L. Chiu and Q. Xue, "Investigation of a wideband 90° hybrid coupler with an arbitrary coupling level," *IEEE Trans. Microw. Theory Techn.*, vol. 58, no. 4, pp. 1022–1029, Apr. 2010.

[11] C.-L. Hsu, J.-T. Kuo, and C.-W. Chang, "Miniaturized dual-band hybrid couplers with arbitrary power division ratios," *IEEE Trans. Microw. Theory Techn.*, vol. 57, no. 1, pp. 149–156, Jan. 2009.

[12] X. Wang, W.-Y. Yin, and K.-L. Wu, "A dual-band coupled-line coupler with an arbitrary coupling coefficient," *IEEE Trans. Microw. Theory Techn.*, vol. 60, no. 4, pp. 945–951, Apr. 2012.

[13] P.-L. Chi, "Miniaturized ring coupler with arbitrary power divisions based on the composite right/left-handed transmission lines," *IEEE Microw. Wireless Compon. Lett.*, vol. 22, no. 4, pp. 170–172, Apr. 2012.

[14] K.-L. Ho and P.-L. Chi, "Miniaturized and large-division-ratio ring coupler using novel transmission-line elements," *IEEE Microw. Wireless Compon. Lett.*, vol. 24, no. 1, pp. 35–37, Jan. 2014.

[15] M.-J. Park and B. Lee, "Design of ring couplers for arbitrary power division with 50 Ω lines," *IEEE Microw. Wireless Compon. Lett.*, vol. 21, no. 4, pp. 185–187, Apr. 2011.

[16] C.-K. Lin and S.-J. Chung, "A compact filtering 180° hybrid," *IEEE Trans. Microw. Theory Techn.*, vol. 59, no. 12, pp. 3030–3036, Dec. 2011.

[17] F. Lin, Q.-X. Chu, and S. W. Wong, "Design of dual-band filtering quadrature coupler using $\lambda/2$ and $\lambda/4$ resonators," *IEEE Microw. Wireless Compon. Lett.*, vol. 22, no. 11, pp. 565–567, Nov. 2012.

[18] Y. S. Wong, S. Y. Zheng, and W. S. Chan, "Quasi-arbitrary phase-difference hybrid coupler," *IEEE Trans. Microw. Theory Techn.*, vol. 60, no. 6, pp. 1530–1539, Jun. 2012.

[19] Y. Wu, J. Shen, and Y. Liu, "Comments on 'quasi-arbitrary phase-difference hybrid coupler'," *IEEE Trans. Microw. Theory Techn.*, vol. 61, no. 4, pp. 1725–1727, Apr. 2013.

[20] Y. Wu, J. Shen, Y. Liu, S.-W. Leung, and Q. Xue, "Miniaturized arbitrary phase-difference couplers for arbitrary coupling coefficients," *IEEE Trans. Microw. Theory Techn.*, vol. 61, no. 6, pp. 2317–2324, Jun. 2013.

[21] S. Y. Zheng, J. H. Deng, Y. M. Pan, and W. S. Chan, "Circular sector patch hybrid coupler with an arbitrary coupling coefficient and phase difference," *IEEE Trans. Microw. Theory Techn.*, vol. 61, no. 5, pp. 1781–1792, May 2013.

[22] E. Gandini, M. Ettorre, R. Sauleau, and A. Grbic, "A lumped-element unit cell for beam-forming networks and its application to a miniaturized Butler matrix," *IEEE Trans. Microw. Theory Techn.*, vol. 61, no. 4, pp. 1477–1487, Apr. 2013.

[23] E. Gandini, M. Ettorre, R. Sauleau, and A. Grbic, "A lumped-element directional coupler with arbitrary output amplitude and phase distributions," in *IEEE MTT-S Int. Microw. Symp. Dig.*, Jun. 2012, pp. 1–3.

[24] J. J. Yao and S. P. Yeo, "Six-port reflectometer based on modified hybrid couplers," *IEEE Trans. Microw. Theory Techn.*, vol. 56, no. 2, pp. 493–498, Feb. 2008.

[25] J. J. Yao, Y. Chen, and S. P. Yeo, "Modifying hybrid coupler design to enhance six-port reflectometer performance," in *Proc. Eur. Microw. Conf.*, Oct. 2005, pp. 256–259.

[26] C.-W. Wang, T.-G. Ma, and C.-F. Yang, "A new planar artificial transmission line and its applications to a miniaturized Butler matrix," *IEEE Trans. Microw. Theory Techn.*, vol. 55, no. 12, pp. 2792–2801, Dec. 2007.

[27] C.-C. Chang, T.-Y. Chin, J.-C. Wu, and S.-F. Chang, "Novel design of a 2.5-GHz fully integrated CMOS Butler matrix for smart-antenna systems," *IEEE Trans. Microw. Theory Techn.*, vol. 56, no. 8, pp. 1757–1763, Aug. 2008.

[28] D. M. Pozar, *Microwave Engineering*. New York, NY, USA: Wiley, 2005.

[29] J.-S. Lim, S.-W. Lee, C.-S. Kim, J.-S. Park, D. Ahn, and S. Nam, "A 4:1 unequal Wilkinson power divider," *IEEE Microw. Wireless Compon. Lett.*, vol. 11, no. 3, pp. 124–126, Mar. 2001.

[30] H.-R. Ahn and S. Nam, "Wideband microstrip coupled-line ring hybrids for high power-division ratios," *IEEE Trans. Microw. Theory Techn.*, vol. 61, no. 5, pp. 1768–1780, May 2013.

Pei-Ling Chi (S'08–M'11) received the B.S. and M.S. degrees in communication engineering from National Chiao Tung University (NCTU), Hsinchu, Taiwan, in 2004 and 2006, respectively, and the Ph.D. degree in electrical engineering from the University of California at Los Angeles (UCLA), Los Angeles, CA, USA, in 2011.

Since 2011, she has been with the National Chiao Tung University, as an Assistant Professor of electrical and computer engineering. She holds several U.S. and international patents in the area of the left-handed metamaterials. Her research interests include the analysis and design of left-handed metamaterial circuits, implementation of microwave components and integrated systems, and development of millimeter-wave/terahertz antennas and communications.

Dr. Chi was the recipient of the Research Creativity Award from the National Science Council, Taiwan, in 2004.

Kuan-Lin Ho received the B.S. degree in electrical and computer engineering and M.S. degree from the Institute of Communications Engineering, National Chiao Tung University (NCTU), Hsinchu, Taiwan, in 2012 and 2014, respectively.

He is currently an Electronic Engineer with Garmin Inc., New Taipei City, Taiwan.